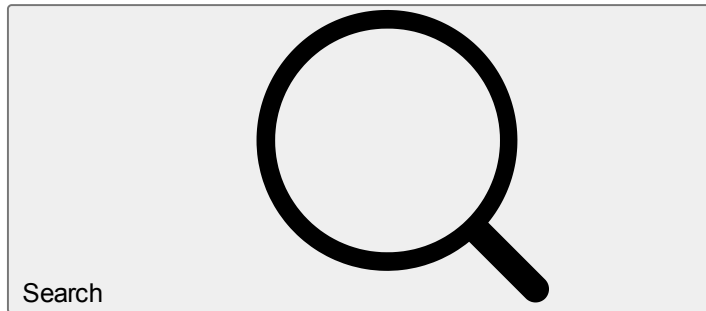


[Skip to main content](#)

Advertisement

 Springer Link

- [Log in](#)

Manufacturing of Photoactive β -Bismuth Oxide by Flame Spray Oxidation[Download PDF](#) ↓[Download PDF](#) ↓

- Peer Reviewed
- [Published: 21 March 2021](#)

Manufacturing of Photoactive β -Bismuth Oxide by Flame Spray Oxidation

- [M. T. Ayala-Ayala](#)^{1,2},
- [M. Y. Ferrer-Pacheco](#)³ &
- [J. Muñoz-Saldaña](#)¹✉

Journal of Thermal Spray Technology volume 30, pages 1107–1119 (2021) [Cite this article](#)

- 260 Accesses
- [Metrics details](#)

Abstract

Photoactive tetragonal bismuth pellets by flame spray oxidation properties of β -Bi₂O₃ keeping collected either from evaporation parameters led to different β -micrometric sized), morphology content quenched in water was feedstock. The obtained powder characteristics of bismuth. Micrometric powder shows the synthesis of snowman-like Bi/ β -Bi₂O₃ Janus particles. The

SPRINGER NATURE

Help us improve your user experience

Would you be willing to answer a few questions about your experience using this site?

[Provide Feedback](#)[No Thanks](#)

nanometric sized Bi_2O_3 powder was continuously obtained by spray oxidation, where its collection efficiency depends on processing parameters and showed spherical morphology and a highly pure tetragonal phase with narrow visible light absorbance ($E_g = 2.26$ eV). These optical characteristics indicate that the obtained β - Bi_2O_3 powder is suitable for high-performance visible-light photocatalyst.

Introduction

During the past decades, bismuth-based oxides, such as perovskites, pyrochlores, Aurivillius, among others have stimulated extensive research related to the preparation, modification, and applications in alternative energies, biomedicine, and environmental remediation (Ref [1,2,3,4,5](#)). Particularly, solutions for environmental remediation taking advantage of the photocatalytic properties of bismuth-based materials are nowadays of big interest.

Bismuth-based semiconducting materials can be excited by visible light irradiation due to their electronic structure and a narrow band gap energy, E_g , which is lower than 3 eV. For instance, bismuth oxide (Bi_2O_3) has received much attention as a potential visible light active photocatalyst for both solar energy conversion and environmental remediation because of its efficient photocatalytic activity, high stability, low cost, and nontoxicity (Ref [6](#)). Its photocatalytic performance is itself closely related to the phase, morphology, structure, size, band gap, surface area, crystallinity, rate of the charge transfer, efficiency of charge separation, among others (Ref [1](#)). The narrow band gap energy of Bi_2O_3 is dependent on its crystal structure (2.2-2.8 eV), which is found in seven polymorphs: low-temperature stable monoclinic α (Ref [7](#)); high-temperature stable fcc δ , and the metastable tetragonal β , bcc γ (Ref [8](#)), orthorhombic ϵ (Ref [9](#)), triclinic ω (Ref [10](#)) and high-pressure hexagonal phases (Ref [11](#)).

The tetragonal β phase has an E_g of ~ 2.3 eV and higher photocatalytic performance than the other Bi_2O_3 polymorphs. β -phase has a unique tunnel structure caused by the special orientation of Bi^{3+} lone electron pairs (LEPs). Its tunnel structure is ideal for the transfer of the photogenerated electrons and holes, preventing their excessive recombination and enabling more free carriers to participate in the photocatalytic process (Ref [12, 13](#)).

It is well known that the physical and chemical and therefore photocatalytic behavior of bismuth-based materials are also strongly dependent on their synthesis method (Ref [14](#)).

The synthesis of β - Bi_2O_3 powder has been reported by several routes that include conventional chemical methods (Ref [15,16,17,18,19](#)) using bismuth nitrates and carbonates as precursors, and alternative physical methods based on the oxidation of granulated bismuth under air or vacuum atmospheres (Ref [20,21,22](#)). For instance, liquid phase microwave irradiation allowed the synthesis of β - Bi_2O_3 nanoparticles with an E_g of 2.77 eV using $\text{Bi}(\text{NO}_3)_3 \cdot 5\text{H}_2\text{O}$ as a precursor. The obtention of yellowish precipitate has been reported to take place under irradiation with 500 W of power for 90 min and then centrifugated and washed several times before drying. This precipitate was finally calcined at 300 °C for 4 h to stabilize the β - Bi_2O_3 (Ref [23](#)).

The hydrothermal process has also been frequently reported for the synthesis of β - Bi_2O_3 powder with specific morphology, e.g., flower-like (Ref [17](#)) or nano-sized sheets (Ref [24](#)). Both methods use consistently $\text{Bi}(\text{NO}_3)_3 \cdot 5\text{H}_2\text{O}$ as a precursor. In the former method, a white suspension was formed by adding acetic acid and ethanol, which was cleared by stirring and adding water. The suspension was then heated at 100 °C for 40 min. The resulting precipitate was washed with deionized water. The hydrothermal process conditions were 100 °C for 24 h in a Teflon stainless autoclave. The autoclave was cooled and heated at 240 °C for 2 h and post-heat treated at 300 °C for 2 h. The band gap energy of 2.48 eV (Ref [25](#)).

SPRINGER NATURE

Help us improve your user experience

Would you be willing to answer a few questions about your experience using this site?

Provide Feedback

No Thanks

It is clear that methods of chemical synthesis of β - Bi_2O_3 powder with interesting morphological characteristics and a narrow band gap energy with high photocatalytic activity for organic pollutants degradation are available in the literature. However, the necessity of an alternative method to synthesize photoactive β - Bi_2O_3 powder in one-step and high volumes with desired physical and chemical properties still exists.

Flame spray is a low-cost, high-performance thermal spray technique typically used to manufacture coatings (Ref 25). The process consists of atomizing particles in a compressed gas that have been melted or are in a semi-molten state thanks to the energy released by a heat source. Combustion between premixed acetylene and oxygen gas provides the energetic jet stream. Particles with velocities below 100 m/s are generally achieved. The lower speed experienced by the in-flight particles compared to other TS techniques can be exploited to increase the particle's dwell time inside the jet, thus improving their temperature (Ref 26). The flame temperature is in the range between 2727 and 3077 °C, where particles only reach, however, 70% of this temperature depending on their residence time in the flame (Ref 25).

Therefore, flame spray oxidation of bismuth seems to be promising to control oxidation characteristics of semimetallic bismuth, the phase transformation of the formed oxides as well on their physicochemical properties. However, the synthesis of highly pure tetragonal bismuth oxide with controlled physical and chemical properties by flame spray is still challenging since the process is highly chaotic. The analysis of process parameters by design of experiments is required seeking to obtain specific particle size distribution, morphology, and phase transformations. Particularly, key factors to stabilize metastable β - Bi_2O_3 at room temperature are dependent on the residence time and intrinsic high cooling rates (Ref 27, 28).

In this work, flame spray oxidation was used to synthesize β - Bi_2O_3 by using bismuth pellets obtained from mineral compounds from Mexico (Ref 29). The structural and microstructural properties of the oxidation products were studied by varying feedstock particle size, and standoff distance (SOD) by a 2^2 factorial design of experiments. Oxidation characteristics of bismuth particles are presented and discussed.

Experimental Methods

Powder Synthesis

Bismuth needle-shaped pellets obtained from mining beneficiation of 1-2 cm in size (Industrias Peñoles SA, Mexico) were used as precursor material and milled in a planetary mill (PM400 Retsch, Hann, Germany) for 30 min using a 10:1 ball to powder ratio at 250 rpm. Milled bismuth powder was classified in fine and coarse particles by sieving, passing through 600, 325, and 140 mesh sieves.

The synthesis of β - Bi_2O_3 was carried out by flame spray oxidation using a 6PII gun (Oerlikon Metco, New York, USA) with a ceramic-type nozzle. 99.999% pure nitrogen gas (Atlas-Copco NPG + SKID plant) was used for particle feeding with a Sulzer Metco 5MPE powder feeder (New York, USA). The combustion atmosphere was fixed for an fuel/oxygen ratio of 1:1.15 ($\text{lmin}^{-1}:\text{lmin}^{-1}$) (acetylene/oxygen) that corresponds to a neutral flame (Ref 30).

The fed powder was heated and oxidized thanks to the energy released during the reaction in the flame spray process, in which the combustion of oxygen and acetylene gases provides the energetic jet stream. The feed rate of bismuth powder was fixed at 18 g/min with high pure nitrogen gas. The SOD and particle size of bismuth varying the SOD and particle size.

The parameters used for the experiments were:

The SOD measured from the nozzle to the substrate of bismuth powder was fixed at 100 mm. The experiments were performed with fine and coarse feedstock powder, respectively. The particles were either evaporated or quenched in water. The particles were collected by condensate and identified as "micrometric sized powder."

SPRINGER NATURE

Help us improve your user experience

Would you be willing to answer a few questions about your experience using this site?

Provide Feedback

No Thanks

Table 1 Flame spray parameters and particle size distribution of the thermal sprayed nanometric and micrometric sized powder

[Full size table](#) >

Structure and Microstructure

Phase identification was performed by XRD with a Rigaku TX, USA Dmax 2100 diffractometer with monochromatic radiation $\text{CuK}\alpha$ ($\lambda = 1.5406 \text{ \AA}$) operating at 30 kV and 20 mA. Diffraction patterns were collected in the range of 20° to 60° of 2θ scale with a 0.02 step size and a step time of 0.5 s with a fixed angle of 5° . Phase quantification was determined by Rietveld refinement using *GSAS*[®] software (Ref [31](#)).

The size distribution of bismuth feedstock was measured using the laser diffractometer (HELOS/BR, Sympatec GmbH, Germany). The technique for measuring the dry powder was REDOS, where samples were placed in the powder feeder and air pressurized at 200 kPa.

Analysis of morphology and particle size distribution of synthesized powder was done by field-emission scanning electron microscopy (FESEM) using a JEOL 7610F microscope (Tokyo, Japan) with secondary electron (SE) detector at 2 kV and backscattering electron (BSE) detector at 15 kV electron acceleration voltage. The cumulative size distribution of flame sprayed powder was determined by *ImageJ*[®] (Ref [32](#)). For each sample, the average particle size was measured in at least 5 micrographs.

The oxidation mechanism of the obtained micrometric powder was analyzed by cross-sectional area of the as-synthesized powder. The powder was embedded in epoxy resin and polished until the particle cross section was observed in an optical microscope. These samples were analyzed with a scanning electron microscope XL30 ESEM-Philips (Massachusetts USA) using energy-dispersive spectroscopy (EDS) for semiquantitative chemical composition characterization. The oxidation characteristics of bismuth were identified by tracking the oxygen distribution with EDS using a backscattering electron detector. The semiquantitative chemical characterization was analyzed with an atomic and mass percentage on at least 3 zones of sample cross sections.

Thermal Transformation Analysis

Phase transitions of commercially available α - Bi_2O_3 powder (Sigma-Aldrich S. de RL. de CV.) have been studied using differential scanning calorimeter/thermogravimeter DSC-TGA (SETSYS Setaram, Caluire-et-Cuire, France). DSC-TGA was run using 70 mg of the powder in platinum crucibles. The heating stage was performed from 400 up to 800 $^\circ\text{C}$ at a rate of 1 $^\circ\text{C}/\text{min}$ in air. The cooling stage was performed from 800 up to 25 $^\circ\text{C}$ varying the cooling rate up to 10 $^\circ\text{C}/\text{min}$.

Optical Properties

UV-VIS NIR spectrophotometry was used to determine the band gap energy of the prepared Bi_2O_3 powder with a Varian spectrophotometer (Cary 5000) coupled to a PTFE integration sphere (Malvern, UK). The band gap was determined by measuring reflectance spectra and using Tauc plot (Eq [1](#)), of the intersection of the extrapolated tangent, which is based on the Kubelk

$$F(R)h\nu = k(h\nu - E_g) \quad (1)$$

where h is the Planck's constant, E_g is the band gap energy (eV) and R is the reflectance and is calculated with

$$F(R) = \frac{(1 - R)^2}{2R}$$

SPRINGER NATURE

Help us improve your user experience

Would you be willing to answer a few questions about your experience using this site?

Provide Feedback

No Thanks

(2)

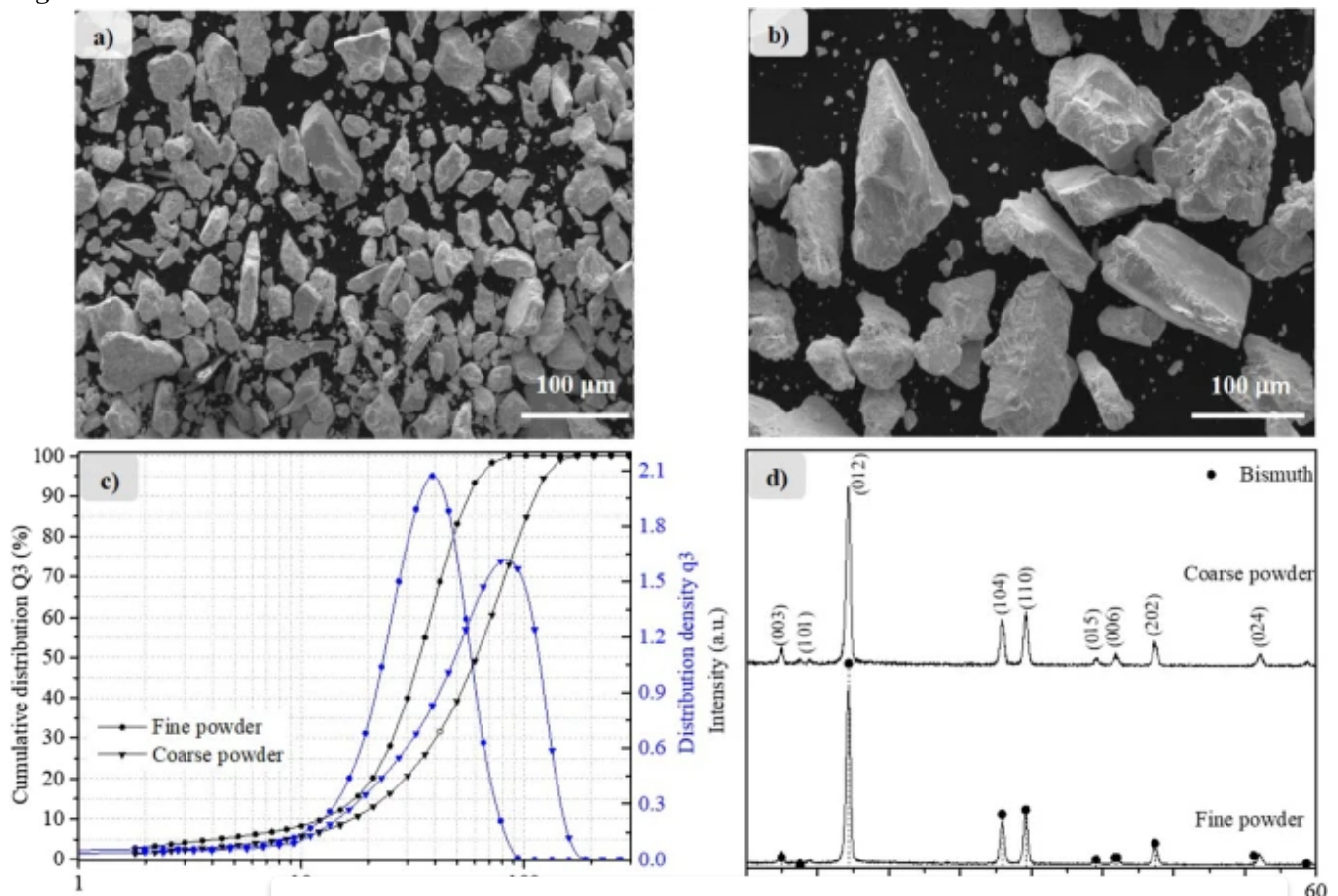
The band gap energy value was obtained by plotting $(F(R)hv)^{1/2}$ versus hv and extrapolating a linear fit to the abscissa axis (Ref 34).

Results and Discussion

Characterization of Precursor Bismuth Powder

As mentioned in the experimental section, bismuth feedstock powder was classified in fine and coarse by milling and sieving with different mesh number. Figure 1(a) and (b) shows the SEM micrographs of both milled powders. The powder morphology is irregular with flat faces and pronounced corners at the edges, which is expected due to the milling process. Figure 1(c) shows the cumulative particle size distribution $Q_3\%$ (black lines) and the distribution density q_3 (blue lines) of both powder types. Fine powder presents a maximum frequency of $38.8 \mu\text{m}$, while the maximum frequency for coarse powder is $78.7 \mu\text{m}$. 90% of the cumulative distribution of fine particles has a maximum size of $60 \mu\text{m}$ and $122 \mu\text{m}$ for coarse particles. Geometry and particle size distribution are relevant characteristics of the fed powder because of its direct influence in energy and mass transfer with the gas flow during the oxidation process.

Fig. 1



SEM micrographs of (a) fine powder and (b) coarse powder, (c) cumulative distribution and (d) X-ray diffraction patterns.

[Full size image](#) >

X-ray diffraction patterns of the powder were identified according to the PDF card for β -Bi₂O₃ hexagonal structure, and space group R-3c.

SPRINGER NATURE

Help us improve your user experience

Would you be willing to answer a few questions about your experience using this site?

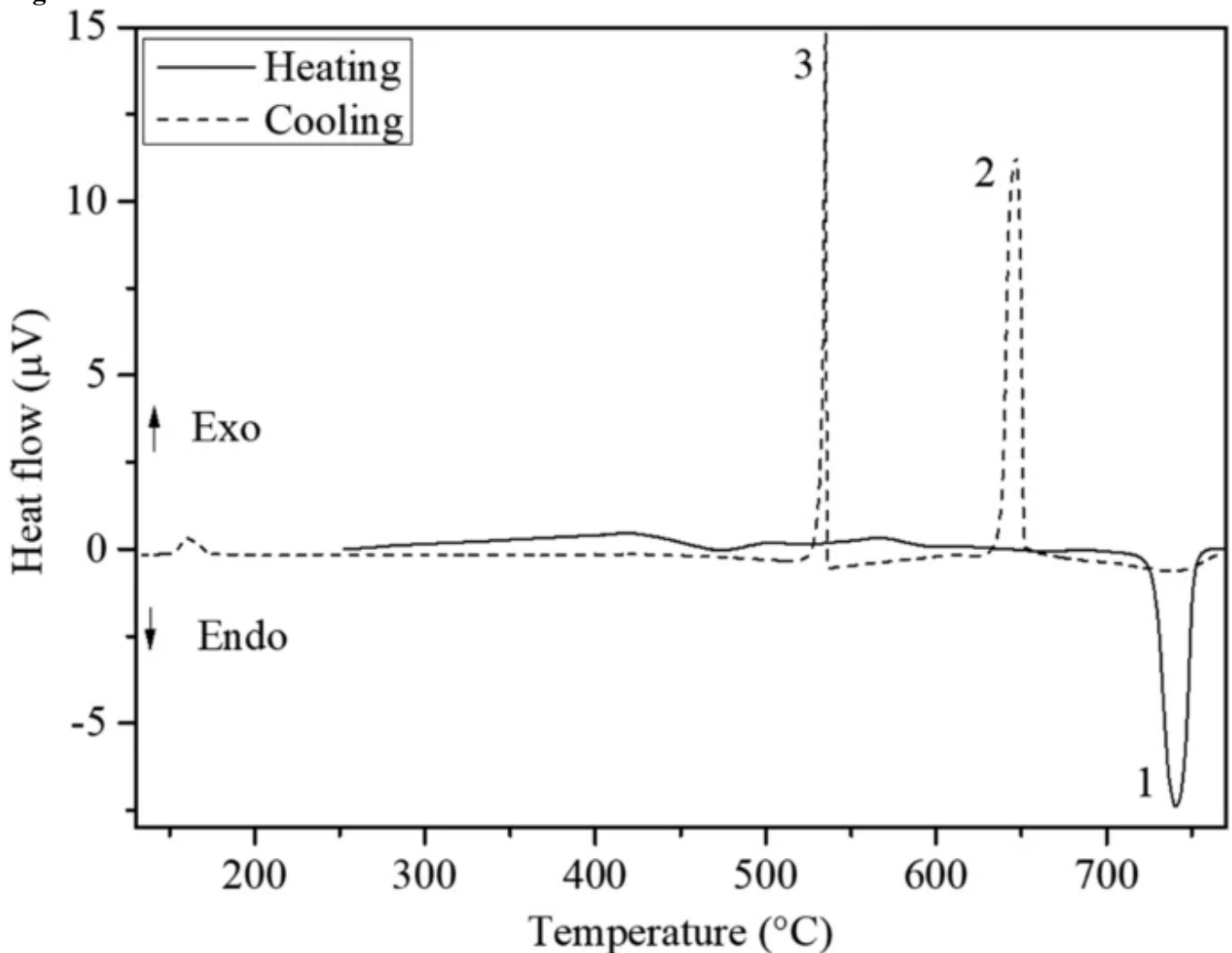
Provide Feedback

No Thanks

Phase Transitions of Bi_2O_3 by DSC

Phase transformations were analyzed in a commercial α - Bi_2O_3 powder by DSC. Figure 2 shows the DSC plot, where positive or negative heat transfer is identified with up and down arrows, which, respectively, correspond to exothermic and endothermic reactions.

Fig. 2



Thermal behavior of α - Bi_2O_3 starting powder

[Full size image](#) >

According to previous data reported elsewhere, two intermediate metastable phases can be obtained by quenching the δ - Bi_2O_3 phase from temperatures between 730 and 823 $^{\circ}\text{C}$. β and γ are present in the range between 667-662 $^{\circ}\text{C}$ and 652-633 $^{\circ}\text{C}$, respectively. The transformations $\delta \rightarrow \beta$ and $\delta \rightarrow \gamma$ depend not only on the chosen atmosphere but also on the used cooling rate (Ref

In the current results, a unique phase was observed during cooling from 800 $^{\circ}\text{C}$ to room temperature. The endothermic peak at 660-630 $^{\circ}\text{C}$ (peak 2) and 530-500 $^{\circ}\text{C}$ (peak 3) can be overlapped. The latter transition is observed at a lower temperature.

The analysis as a function of cooling rate is used to determine the metastable state if high cooling

SPRINGER NATURE

Help us improve your user experience

Would you be willing to answer a few questions about your experience using this site?

Provide Feedback

No Thanks

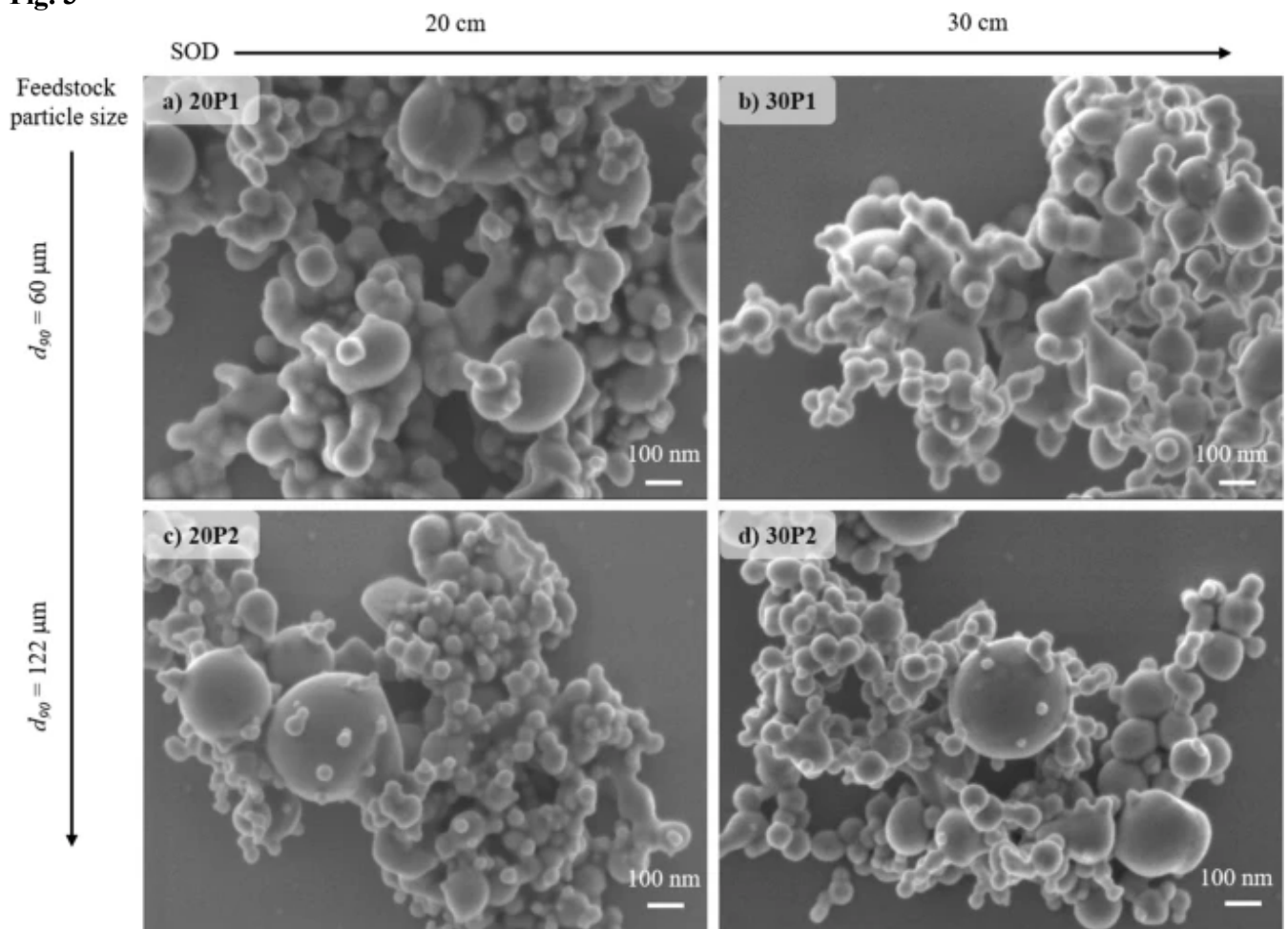
Based on these results, it is possible to envisage retaining the β - Bi_2O_3 by flame spray if abrupt cooling (high cooling rates) from temperatures above $650\text{ }^\circ\text{C}$ is undertaken, which can be easily achieved by collecting evaporated or water quenched in-flight particles.

Thermally sprayed oxidized powder was collected in two ways, from evaporated particles and quenched in water inferring two mechanisms of bismuth oxidation. Bigger particles dropped into the water leading to partial oxidation, whereas, a certain number of fine particles evaporated and were completely oxidized due to the high temperature of the flame.

Characterization of Nanometric-Sized Bismuth Oxide Powder

The evaporated powder presents a characteristic bright yellowed color and nanometric particle size. This powder was labeled as “nanometric” and its physicochemical properties were as follows. Figure 3 shows typical SEM micrographs recorded at high magnifications of the nanometric powder obtained by varying the SOD and particle size of feedstock powder.

Fig. 3



SEM micrographs for

[Full size image](#) >

The synthesized powder shows particles around 100 nm and few bigger ones observed in samples 20P1 and 30P1. The bigger particles have a large effective agglomeration.

SPRINGER NATURE

Help us improve your user experience

Would you be willing to answer a few questions about your experience using this site?

Provide Feedback

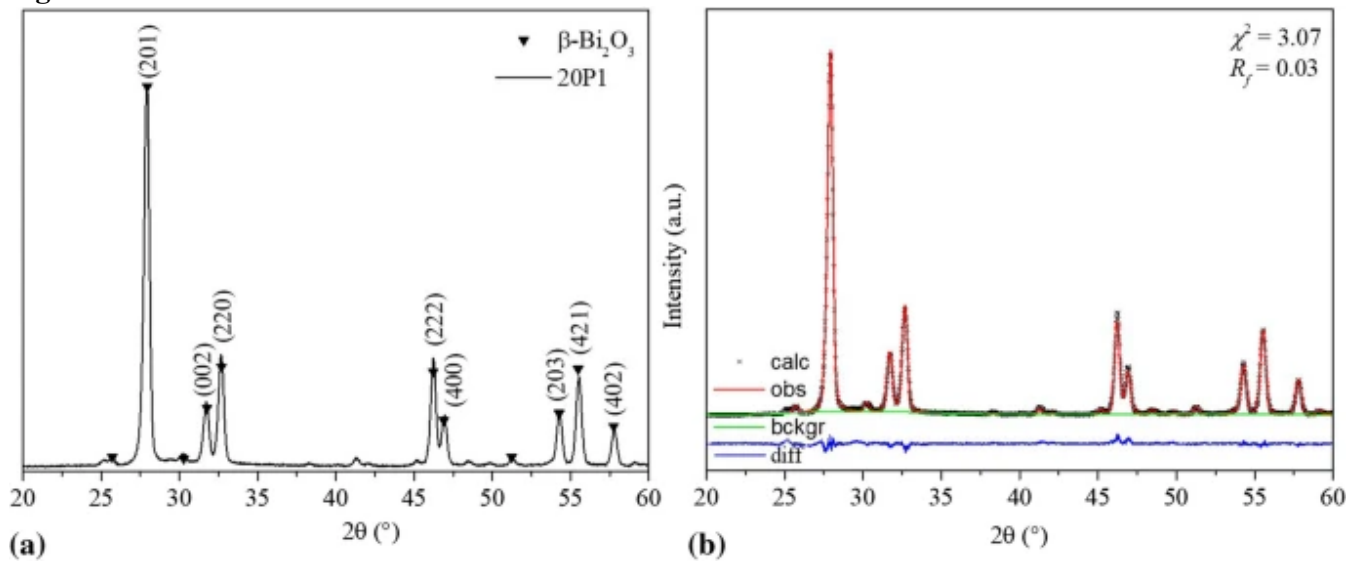
No Thanks

The cumulative size distribution of this powder is shown in Table 1. For each sample, at least 5 micrographs were measured reporting the average particle size. The 90% (d_{90}) of the cumulative distribution of nanometric particles has a maximum size between 227 and 163 nm for fine feedstock powder and 188–133 nm for coarse powder.

An increase in the SOD decreases the size of the nanometric oxidized powder (see d_{90} in Table 1). Additionally, an increase in the size of feedstock powder decreases the size of the nanometric oxidized powder. Specifically, fine *P1* feedstock generated agglomerates of nanometric sized particles, which are larger than those obtained with coarse *P2* feedstock.

X-ray diffraction and Rietveld refinement patterns of as-synthesized powder are shown in Fig. 4. A typical XRD pattern of *20P1* sample is shown in Fig. 4(a). All samples exhibit a high pure Bi_2O_3 phase with a tetragonal structure. No evidence of secondary phases or impurities was observed. All diffraction lines can be indexed to a tetragonal phase with $a = b = 7.742 \text{ \AA}$, $c = 5.631 \text{ \AA}$ unit cell parameters identified with PDF 27-0050 with a space group $P421-c$.

Fig. 4



(a) X-ray diffraction and (b) Rietveld refined patterns of nanometric sized thermal sprayed $\beta\text{-Bi}_2\text{O}_3$ powder

[Full size image](#) >

Rietveld refinement allowed us to calculate the structural parameters of as-synthesized powder. Figure 4(b) shows the refined pattern of *20P1* sample. The calculated lattice parameters are $a = b = 7.7405 \text{ \AA}$ and $c = 5.6328 \text{ \AA}$, which are in good agreement with theoretical values. The goodness coefficient (χ^2) and the structural factor (R_f) are 3.07 and 0.03, respectively, which represent the refinement quality (Fig. 4b). The R_f -value suggests an excellent relationship between the calculated model and the experimental XRD pattern.

The optical absorption characteristics of the as-synthesized Bi_2O_3 measured respective to its band gap energy are

shown in Fig. 5. The band gap corresponds to Tauc plot (Eq. method based on the Kubelk. Bi_2O_3 by extrapolating the Bi_2O_3 powder possess a band range of the solar spectrum for photocatalytic applications. This oxide with a nanometric spher

Figure 5

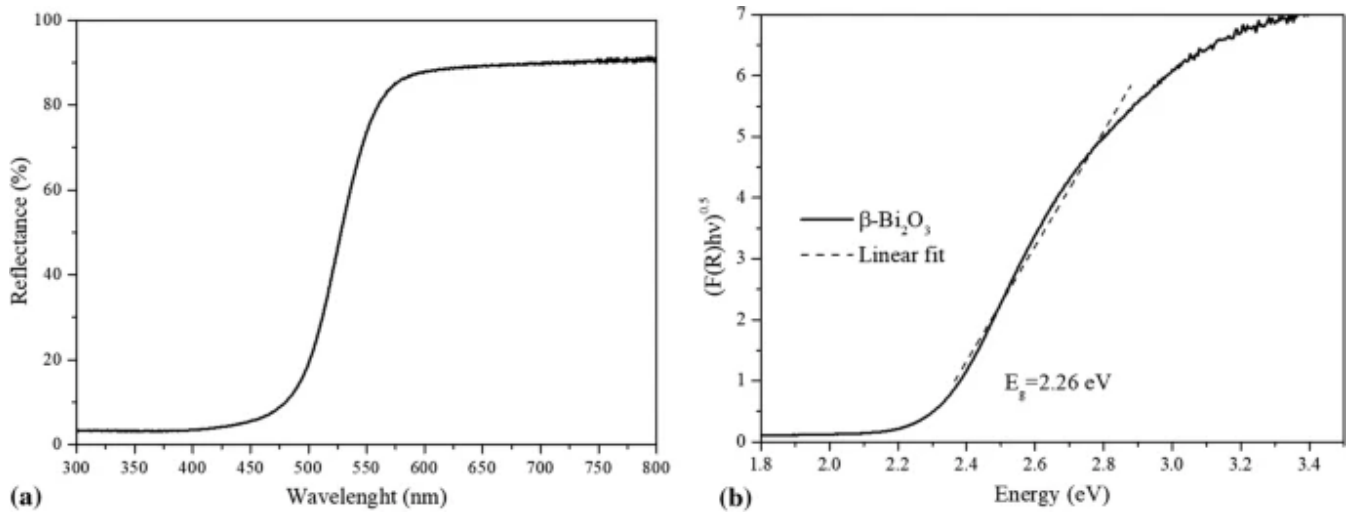
SPRINGER NATURE

Help us improve your user experience

Would you be willing to answer a few questions about your experience using this site?

Provide Feedback

No Thanks



(a) Reflectance spectra and (b) Tauc plot to determine the indirect band gap energy of β - Bi_2O_3

[Full size image](#) >

Characterization of Micrometric-Sized Bismuth Oxidized Powder

The quenched powder (collected in water) was labeled as “micrometric” and can be distinguished by a dark green color.

The morphology of the micrometric sized oxidized powder recorded with a BSE detector is shown in Fig. 6. The micrometric powder showed particles with a rough surface and an approximately spherical morphology joined to the hemispheres of other smaller particles. Molten in-flight particles collided with each other leading to particular agglomeration features between few elements leading to the formation of the so-called snowman-like morphology (Ref 36, 37). These particles show different colors, associated with at least two different phases. Clear zones Z_1 correspond to bismuth while the dark zones Z_2 are bismuth oxides (see arrows from Fig. 6c) according to their molecular weight. Samples 20P1 and 30P1 (Fig. 6a and b, respectively) present smaller particles $< 50 \mu\text{m}$ compared to samples 20P2 and 30P2 $> 50 \mu\text{m}$ (Fig. 6c and d, respectively).

Fig. 6

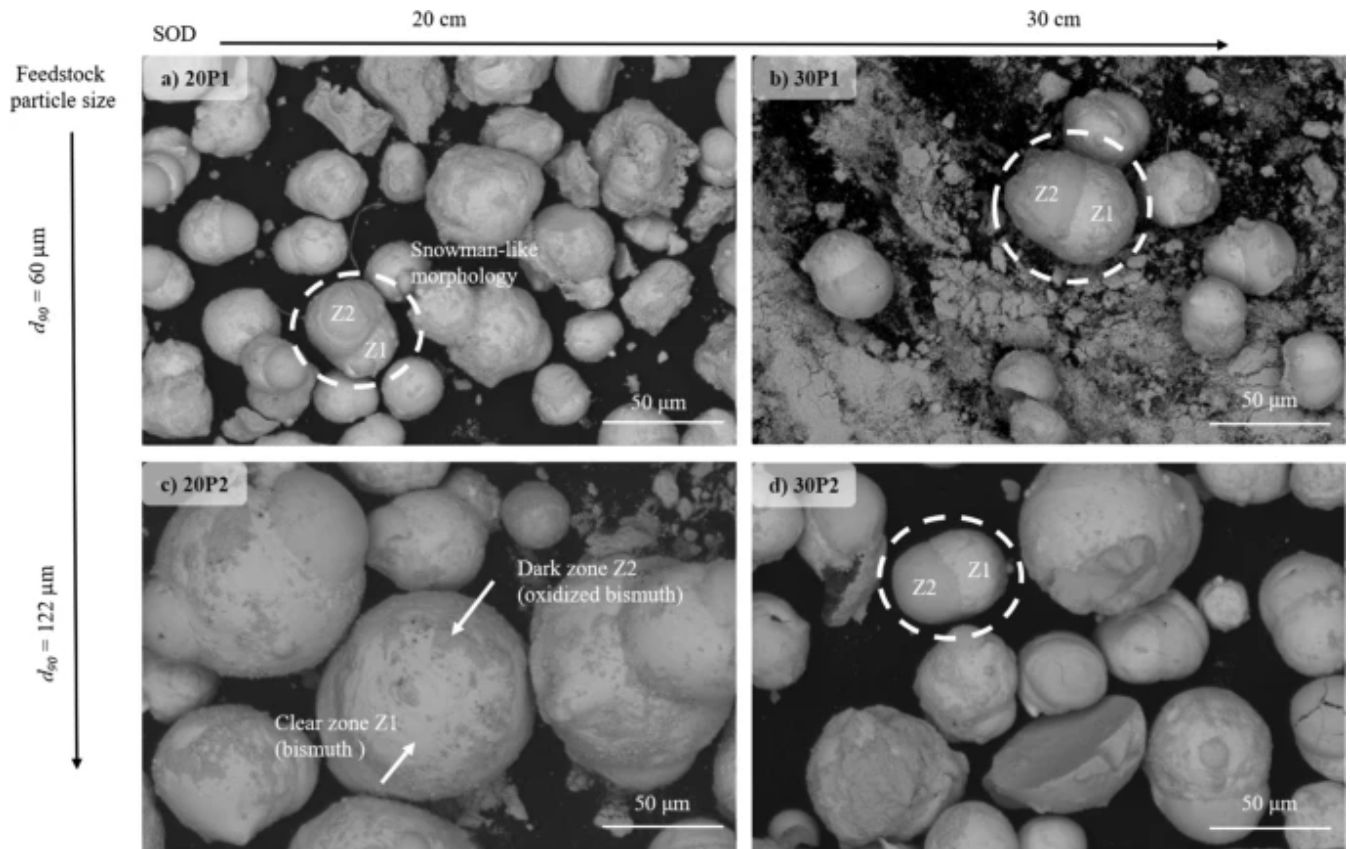
SPRINGER NATURE

Help us improve your user experience

Would you be willing to answer a few questions about your experience using this site?

Provide Feedback

No Thanks



SEM micrographs of micrometric sized thermal sprayed β - Bi_2O_3 powder

[Full size image](#) >

Table 1 shows the cumulative size distribution of the micrometric oxidized powder. The size of this powder decreases as the SOD distance increases. The d_{90} of this powder using fine *P1* feedstock is 37 μm and 33 μm for SOD of 20 cm and 30 cm, respectively. In the case of coarse *P2* feedstock, the d_{90} size is 68 μm and 64 μm for SOD of 20 cm and 30 cm, respectively. Thus, the size of the obtained powder directly depends on the size of the feedstock material and is inversely proportional to the SOD distance, i.e., the size of the obtained micrometer powder decreases as the spray distance increases.

A change in the morphology and size of the feedstock powder is expected to take place interacting with the flame spray. It is well known, that the shape changes from irregular/angular morphology to a spherical shape (droplets formation) due to the flame process (Ref 25). The particles are subject to conductive heat transfer and become spherical after reaching their melting point (271 $^{\circ}\text{C}$) while passing through the flame. All particles exhibit rough surfaces generated due to the quenching into cool water and in some cases address fractures because of the thermal shock. During the in-flight, the particles start evaporating (1564 $^{\circ}\text{C}$) after reaching their melting point, where the amount of evaporated mass depends on the size, thermal conductivity, speed, and trajectory followed by each particle, leading to a decrease in size of the oxidized particles (Ref 25).

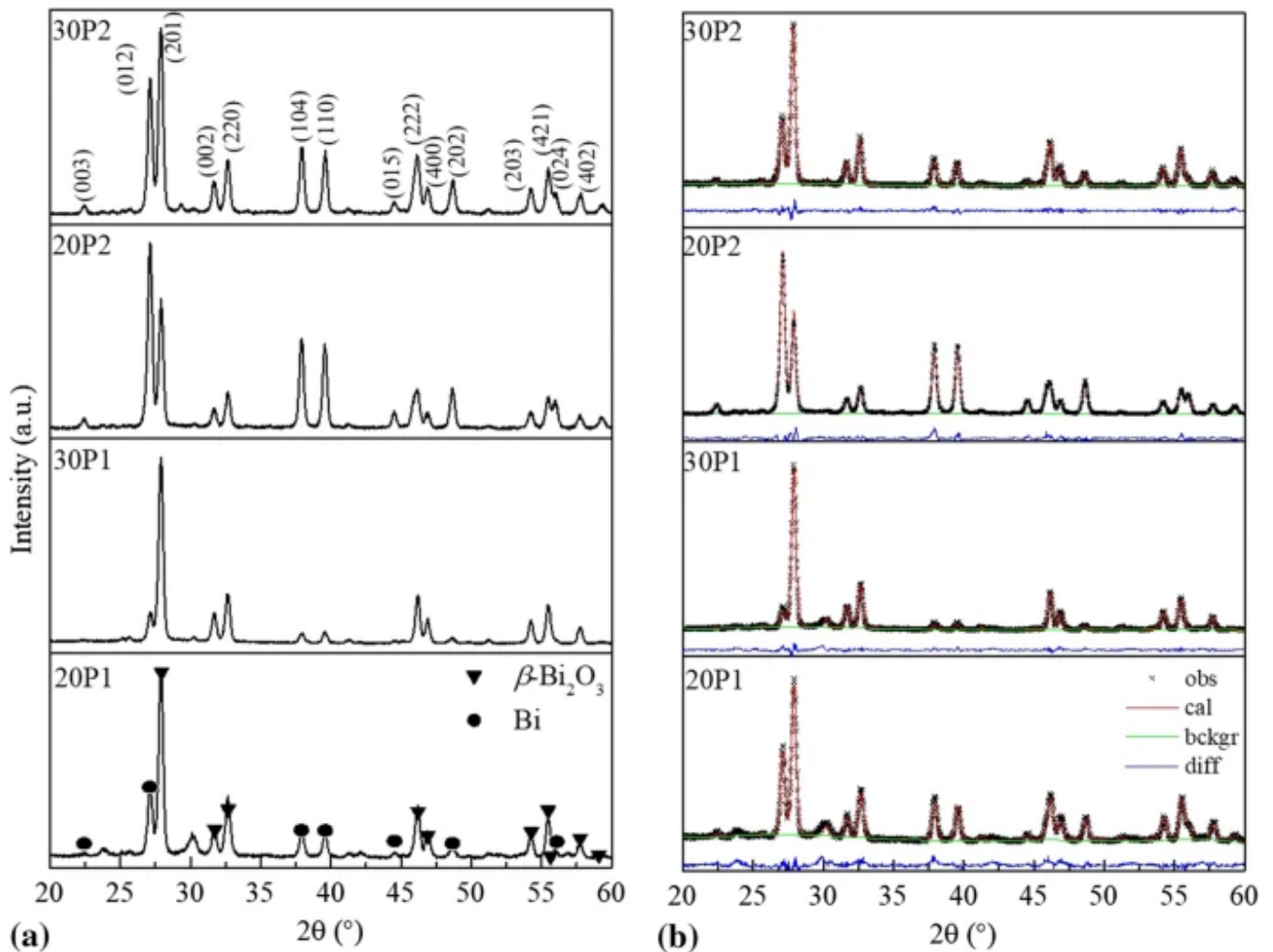
X-ray diffraction patterns of r identified with PDF 44-1246. Moreover, samples 20*P1* and at 27.9 $^{\circ}$ of 2 θ .

Fig. 7

SPRINGER NATURE

Help us improve your user experience

Would you be willing to answer a few questions about your experience using this site?



(a) X-ray diffraction and (b) Rietveld refined patterns of micrometric sized thermal sprayed bismuth oxidized powder

[Full size image](#) >

Rietveld refinement was done to all x-ray patterns to quantify the phase content of samples and evaluate the effect of the flame spray process on the structure of bismuth oxide (Fig. 7b). Each refinement is composed by four curves: (a) the experimental patterns (shown in black), (b) the adjusted patterns (red), (c) the adjusted background to calculate the phase content and lattice parameters (green) and d) the error line (blue) generated from the difference between the experimental and adjusted patterns. The obtained χ^2 and R_f were 3 and 0.1, respectively (Table 2). The quantification confirmed that samples prepared with fine feedstock powder (sample 20P1 and 30P1) exhibit a higher content of β - Bi_2O_3 77% and 91%, respectively. The increase in SOD generates an increase in the amount of oxidized bismuth, which was consistently observed for fine and coarse feedstock powder.

Table 2 Structural parameters of micrometric sized thermal sprayed powder obtained from Rietveld refinement

[Full size table](#) >

In all samples, the lattice para
30P1 sample presents the hig
exhibits enhanced electron tra
mentioned before, the unique
be associated with its exceller
photogenerated electrons and
participate in the photodecon

SPRINGER NATURE

Help us improve your user experience

Would you be willing to answer a few questions about your experience using this site?

Provide Feedback

No Thanks

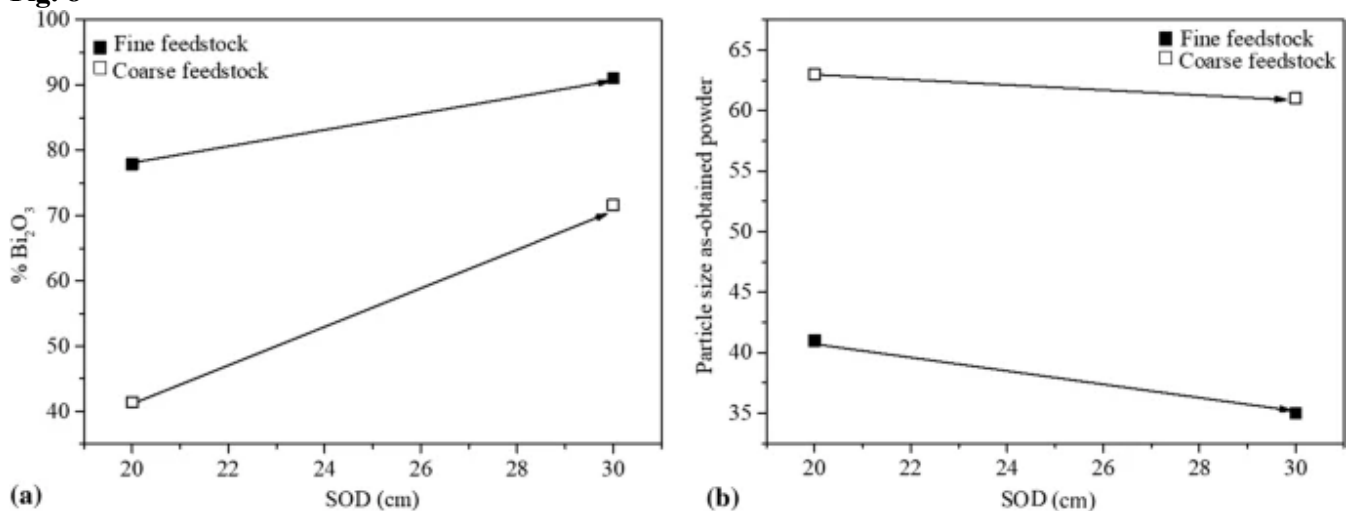
It is worth mentioning that the physicochemical characteristics of this powder make it suitable to be used in spraying deposition processes, e.g., by cold spray.

Influence of Flame Spray Parameters on Oxidation Characteristics of Bismuth

The influence of thermal spray parameters is evidenced in the content of bismuth oxide. As mentioned before, a smaller feedstock size leads to a higher oxidation content. If the particle possesses a smaller diameter the heat transfer from the surface onto the core is favorable and the oxidation process is promoted. A similar effect is obtained with longer standoff distances. The residence time of the in-flight particle in the flame increases by increasing the SOD. The particle is surrounded by oxidant gas for a longer time. Smaller particles have a higher surface area which maximizes the total content of formed bismuth oxide. Under these conditions, bismuth coarse powder does not completely oxidize due to its big size. The low surface area carries out poor contact with oxygen molecules. Moreover, the residence time of the in-flight particles in the heat zone of the flame is not enough to reach a melting state diminishing the conditions promoting oxidation (Ref [25](#), [30](#)).

For the sake of clarity, the effect of flame spray parameters, feedstock size, and SOD combinations on the oxidation of bismuth and the size of the micrometric as-synthesized powder is shown in Fig. [8](#). This figure provides a good summary of previously described effects, where the formation of β - Bi_2O_3 is promoted by using fine bismuth feedstock powder and small SOD (Fig. [8a](#)). The same effect is evidenced in the synthesis of small micrometric β - Bi_2O_3 particles (Fig. [8b](#)). This analysis agrees with the literature that establishes that oxidation of particles increases with the temperature, a higher residence time of in-flight particles in the flame by increasing SOD and with an adequate size of feedstock powder.

Fig. 8



Effect of SOD and feedstock particle size on the (a) phase content of β - Bi_2O_3 and (b) particle size of micrometric sized thermal sprayed powder

[Full size image](#) >

Oxidation Mechanism

Figure [9](#) shows the oxidation cross-sectional area of as-synthesized samples. The heterointerface of two phases in the $30PI$ sample, where two micrometric composite shows the coexistence measured from EDS analysis

Fig. 9

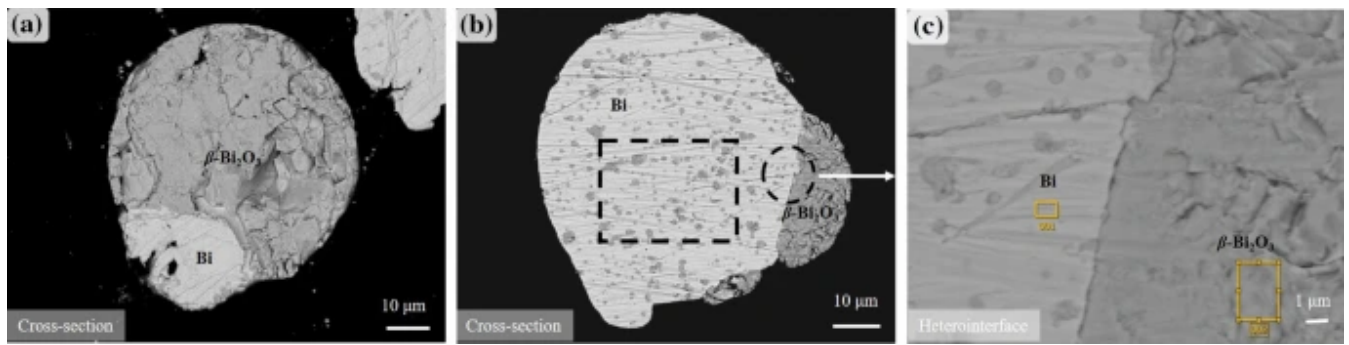
SPRINGER NATURE

Help us improve your user experience

Would you be willing to answer a few questions about your experience using this site?

Provide Feedback

No Thanks



(a, b) SEM micrographs of particle cross sections for 30P1 and 30P2 samples, respectively, and (c) heterointerface area between Bi/ β -Bi₂O₃

[Full size image](#) >

Sample 30P2 (Fig. 9b) shows a similar heterointerface between bismuth (clear zone) and bismuth oxide (dark zone). Whereas, the oxidation mechanism is the opposite than 30P1 sample since the snowman-like particle possesses a higher content of bismuth than bismuth oxide. Although, the semisphere of bismuth is partially oxidized on its core.

Regarding the heterointerface between Bi and β -Bi₂O₃, the inset of Fig. 9(c) shows a magnification of a 30P2 particle interface. This micrograph evidences the formation of a composite sharing different compositions in a heterogeneous interface between a metal and a metal oxide Bi/ β -Bi₂O₃.

These composites are usually classified as Janus particles and have a particular shape and surface chemistry showing different physical and chemical properties (Ref 37). Janus particles may show different magnetic, electrical, semiconductive, optical, optoelectronic, and catalytic properties (Ref 36). Due to the nature of as-synthesized snowman-like Bi/ β -Bi₂O₃ Janus particles, the photocatalytic properties of Bi₂O₃ are expected to be enhanced because of the interfacial interactions originated from electron transfer across the interface. It has been reported that Bi₂O₃ shows an enhancement in its photocatalytic activity by depositing metallic particles to serve as electron scavenger to decrease photorecombination of the electron-hole photogeneration and then induce charge separation to carry out redox reactions with pollutants (Ref 40,41,42,43). Electrodes of Bi/ β -Bi₂O₃ have shown stronger visible light absorption and high photoactivity for hydrogen generation due to the electron transfer from Bi to β -Bi₂O₃ (Ref 44). The current as-synthesized micrometric snowman-like Bi/ β -Bi₂O₃ Janus particles are a promising candidate for photocatalytic applications.

The obtained powder with 30P2 conditions kept the snowman morphology but showed as expected different oxidation characteristics. An internally partially oxidized big bismuth particle appears attached to a smaller one (see Fig. 9b). This behavior can be explained based on the heat transfer mechanism that takes place immediately after the particles interact with the hot gas, where they are heated from the surface to their nuclei. The kinetic of this process depends on several parameters, such as size and particle trajectory inside the flame, thermal conductivity, etc. Small particles (P1) get uniformly heated and reach faster conditions of fusion, vaporization, with the simultaneous oxidation process. On the opposite, bigger particles (P2) have intrinsically lower kinetics leading to an overall lower oxide content.

Heat and mass transfer play a following expression describe (Ref 30):

$$Q = h (\pi d_p^2) (T_\infty - T_s) \quad (3)$$

where d_p and T_s are the diam temperature of hot gas and th

SPRINGER NATURE

Help us improve your user experience

Would you be willing to answer a few questions about your experience using this site?

Provide Feedback

No Thanks

($5.67 \times 10^{-8} \text{ W/m}^2\text{K}^4$, h is the heat transfer coefficient between the hot gas and the particle and expressed in terms of the Nusselt number (Nu) defined in Eq 4 (Ref 25, 30):

$$Nu = \frac{hd_p}{\kappa} \quad (4)$$

where κ is the thermal conductivity of the gas.

For a particle to reach a uniform temperature, it is required that its thermal conductivity κ_p is higher than the κ of the gas, described as the Biot number $Bi = \kappa/\kappa_p$ and should be $Bi < 0.01$ (Ref 25, 30).

A schematic representation of the oxidation mechanism that corresponds to an in-flight particle oxidized by combustion thermal spray as described elsewhere (Ref 25) can be adapted to the current results. In the referred figure, the oxidation mechanism of an in-flight particle interacting with hot gas depends on the heat transfer processes and the size of feedstock powder. Under melting and/or evaporation conditions, oxidation of the particles takes place and their diameter naturally decreases inside the flame plume, which is a time-dependent process influenced by their trajectory within the heat zone (Ref 30).

Conclusions

Controlling flame spraying parameters (standoff distance, flame temperature, Bi-powder morphology, and size) allows the synthesis of photoactive tetragonal bismuth oxide powder with nanometric and micrometric sizes. Morphology of micrometric sized powder corresponds to Janus particles of a Bi/ β - Bi_2O_3 snowman-like morphology, where the heterostructure potentially allows the electron transfer between a semiconductor (β - Bi_2O_3) and an electron scavenger (Bi). This powder is ready to be used in spraying deposition processes, e.g., by cold spray. The obtained nanometric sized powder corresponds to highly pure β - Bi_2O_3 , which is highly photoactive with a band gap energy $E_g = 2.26 \text{ eV}$.

References

1. 1.

H. Zhao, F. Tian, R. Wang, and R. Chen, A Review on Bismuth-Related Nanomaterials for Photocatalysis, *Rev. Adv. Sci. Eng.*, 2014, **3**(1), p 3-27. <https://doi.org/10.1166/rase.2014.1050>

[Article](#) [Google Scholar](#)

2. 2.

D.A. Fernandez-Benavides, A.I. Gutierrez-Perez, A.M. Benitez-Castro, M.T. Ayala-Ayala, B. Moreno-Murguia, and J. Muñoz-Saldaña, Comparative Study of Ferroelectric and Piezoelectric Properties of BNT-BKT-BT Ceramics near the Phase Transition Zone. *Materials (Basel)*, 2018, **11**(3), p 2-16.

<https://doi.org/10.3390>

[CAS](#) [Article](#) [Google](#)

3. 3.

D.A. Fernández-Benavides, J. Muñoz-Saldaña, A Novel Bismuth Oxide Nanopowder for Photocatalysis: Synthesis, Characterization and Quantification, *Sens. Actuators B*

[CAS](#) [Article](#) [Google](#)

SPRINGER NATURE

Help us improve your user experience

Would you be willing to answer a few questions about your experience using this site?

Provide Feedback

No Thanks

4. 4.

M. Esquivel-Gaon, S. Anguissola, D. Garry, A.D.C. Gallegos-Melgar, J.M. Saldaña, K.A. Dawson, A. De Vizcaya-Ruiz, and L.M. Del Razo, Bismuth-Based Nanoparticles as the Environmentally Friendly Replacement for Lead-Based Piezoelectrics, *RSC Adv.*, 2015, **5**(35), p 27295-27304.

[CAS](#) [Article](#) [Google Scholar](#)

5. 5.

T. Jardiel, A.C. Caballero, and M. Villegas, Aurivillius Ceramics: Bi₄Ti₃O₁₂-Based Piezoelectrics, *J. Ceram. Soc. Jpn.*, 2008, **116**, p 511-518.

[CAS](#) [Article](#) [Google Scholar](#)

6. 6.

M. Mehring, From Molecules to Bismuth Oxide-Based Materials: Potential Homo- and Heterometallic Precursors and Model Compounds, *Coord. Chem. Rev.*, 2007, **251**(7-8), p 974-1006.

<https://doi.org/10.1016/j.ccr.2006.06.005>

[CAS](#) [Article](#) [Google Scholar](#)

7. 7.

G. Malmros, The Crystal Structure of Alpha-Bi₂O₃, *Acta Chem. Scand.*, 1970

<https://doi.org/10.3891/acta.chem.scand.24-0384>

[Article](#) [Google Scholar](#)

8. 8.

H.A. Harwig, On the Structure of Bismuthsesquioxide: The Alpha, Beta, Gamma and Delta-Phase, *Z. Anorg. Allg. Chem.*, 1978, **444**, p 151-166. <https://doi.org/10.1090/gsm/146/03>

[CAS](#) [Article](#) [Google Scholar](#)

9. 9.

N. Cornei, N. Tancret, F. Abraham, and O. Mentré, New ϵ -Bi₂O₃ Metastable Polymorph, *Inorg. Chem.*, 2006, **45**(13), p 4886-4888. <https://doi.org/10.1021/ic0605221>

[CAS](#) [Article](#) [Google Scholar](#)

10. 10.

A.F. Gualtieri, S. Immo
Compound ω -Bi₂O₃,

[CAS](#) [Article](#) [Google](#)

11. 11.

S. Ghedia, T. Lochere
Temperature Multianvi
Properties, *Phys. Rev.*

[CAS](#) [Article](#) [Google Scholar](#)

SPRINGER NATURE

Help us improve your user experience

Would you be willing to answer a few questions about your experience using this site?

Provide Feedback

No Thanks

12. 12.

A.L.J. Pereira, O. Gomis, J.A. Sans, J. Contreras-García, F.J. Manjón, P. Rodríguez-Hernández, A. Muñoz, and A. Beltrán, β -Bi₂O₃ under Compression: Optical and Elastic Properties and Electron Density Topology Analysis, *Phys. Rev. B*, 2016, **93**(22), p 1-13. <https://doi.org/10.1103/PhysRevB.93.224111>

[CAS](#) [Article](#) [Google Scholar](#)

13. 13.

A.L.J. Pereira, J.A. Sans, R. Vilaplana, O. Gomis, F.J. Manjón, P. Rodríguez-Hernández, A. Muñoz, C. Popescu, and A. Beltrán, Isostructural Second-Order Phase Transition of β -Bi₂O₃ at High Pressures: An Experimental and Theoretical Study, *J. Phys. Chem. C*, 2014, **118**(40), p 23189-23201.

<https://doi.org/10.1021/jp507826j>

[CAS](#) [Article](#) [Google Scholar](#)

14. 14.

X. Meng, and Z. Zhang, Bismuth-Based Photocatalytic Semiconductors: Introduction, Challenges and Possible Approaches, *J. Mol. Catal. A Chem*, 2016, **423**, p 533-549. <https://doi.org/10.1016/j.molcata.2016.07.030>

[CAS](#) [Article](#) [Google Scholar](#)

15. 15.

M. Schlesinger, S. Schulze, M. Hietschold, and M. Mehring, Metastable β -Bi₂O₃ Nanoparticles with High Photocatalytic Activity from Polynuclear Bismuth Oxido Clusters, *Dalt. Trans.*, 2013, **42**(4), p 1047-1056.

<https://doi.org/10.1039/c2dt32119j>

[CAS](#) [Article](#) [Google Scholar](#)

16. 16.

L. Liu, J. Jiang, S. Jin, Z. Xia, and M. Tang, Hydrothermal Synthesis of β -Bismuth Oxide Nanowires from Particles, *CrystEngComm*, 2011, **13**(7), p 2529-2532. <https://doi.org/10.1039/c0ce00773k>

[CAS](#) [Article](#) [Google Scholar](#)

17. 17.

J. Wang, X. Yang, K. Zhao, P. Xu, L. Zong, R. Yu, D. Wang, J. Deng, J. Chen, and X. Xing, Precursor-Induced Fabrication of β -Bi₂O₃ Microspheres and Their Performance as Visible-Light-Driven Photocatalysts, *J. Mater. Chem. A*, 2013, **1**(32), p 9069-9074. <https://doi.org/10.1039/c3ta11652b>

[CAS](#) [Article](#) [Google Scholar](#)

18. 18.

H.Y. Jiang, P. Li, G. Li, Stabilized by Surface-
<https://doi.org/10.1039/c0ce00773k>

[CAS](#) [Article](#) [Google Scholar](#)

19. 19.

SPRINGER NATURE

Help us improve your user experience

Would you be willing to answer a few questions about your experience using this site?

T. Selvamani, S. Anandan, L. Granone, D.W. Bahnemann, and M. Ashokkumar, Phase-Controlled Synthesis of Bismuth Oxide Polymorphs for Photocatalytic Applications, *Mater. Chem. Front. R. Soc. Chem.*, 2018, **2**(9), p 1664-1673. <https://doi.org/10.1039/c8qm00221e>

[CAS](#) [Article](#) [Google Scholar](#)

20. 20.

H.X. Hu, K.Q. Qiu, and G.F. Xu, Preparation of Nanometer δ - and β -Bismuth Trioxide by Vacuum Vapor-Phase Oxidation, *Trans. Nonferrous Met. Soc. China (English Ed.)*, 2006, **16**(1), p 173-177.

[https://doi.org/10.1016/S1003-6326\(06\)60031-9](https://doi.org/10.1016/S1003-6326(06)60031-9)

[CAS](#) [Article](#) [Google Scholar](#)

21. 21.

L. Kumari, J.H. Lin, and Y.R. Ma, Synthesis of Bismuth Oxide Nanostructures by an Oxidative Metal Vapour Phase Deposition Technique, *Nanotechnology*, 2007, **18**(29), p 7. <https://doi.org/10.1088/0957-4484/18/29/295605>

<https://doi.org/10.1088/0957-4484/18/29/295605>

[CAS](#) [Article](#) [Google Scholar](#)

22. 22.

E. Diez, O. Monnereau, L. Tortet, G. Vacquier, P. Llewellyn, and F. Rouquerol, Synthesis of Bismuth (III) Oxide from Oxalate: A Study by Controlled Transformation Rate Thermal Analysis (CRTA), *J. Optoelectron. Adv. Mater.*, 2000, **2**(5), p 552-556.

[CAS](#) [Google Scholar](#)

23. 23.

Q. Huang, S. Zhang, C. Cai, and B. Zhou, β - and α -Bi₂O₃ Nanoparticles Synthesized via Microwave-Assisted Method and Their Photocatalytic Activity towards the Degradation of Rhodamine B, *Mater. Lett.*, 2011, **65**(6), p 988-990. <https://doi.org/10.1016/j.matlet.2010.12.055>

[CAS](#) [Article](#) [Google Scholar](#)

24. 24.

J. Hou, C. Yang, Z. Wang, W. Zhou, S. Jiao, and H. Zhu, In Situ Synthesis of α - β Phase Heterojunction on Bi₂O₃ Nanowires with Exceptional Visible-Light Photocatalytic Performance, *Appl. Catal. B Environ.*, 2013, **142-143**, p 504-511. <https://doi.org/10.1016/j.apcatb.2013.05.050>

[CAS](#) [Article](#) [Google Scholar](#)

25. 25.

L. Pawlowski, *The Sci*

[Book](#) [Google Scholar](#)

26. 26.

F. Fanicchia, D.A. Axi
CoNiCrAlY & YSZ C

<https://doi.org/10.1016/j.surfcoat.2017.01.019>

SPRINGER NATURE

Help us improve your user experience

Would you be willing to answer a few questions about your experience using this site?

Provide Feedback

No Thanks

[CAS](#) [Article](#) [Google Scholar](#)

27. 27.

H.A. Harwig, and A.G. Gerards, The Polymorphism of Bismuth Sesquioxide, *Thermochim. Acta*, 1979, **28**(1), p 121-131. [https://doi.org/10.1016/0040-6031\(79\)87011-2](https://doi.org/10.1016/0040-6031(79)87011-2)

[CAS](#) [Article](#) [Google Scholar](#)

28. 28.

H.A. Harwig, and J.W. Weenk, Phase Relations in Bismuthsesquioxide, *ZAAC J. Inorg. Gen. Chem.*, 1978, **444**(1), p 167-177. <https://doi.org/10.1002/zaac.19784440119>

[CAS](#) [Article](#) [Google Scholar](#)

29. 29.

A.V. Naumov, World Market of Bismuth: A Review, *Metall. Rare Noble Met.*, 2007, **48**(1), p 13-19. <https://doi.org/10.3103/S1067821207010038>

[Article](#) [Google Scholar](#)

30. 30.

P.L. Fauchais, J.V.R. Heberlein, and M.I. Boulos, *Thermal Spray Fundamentals: From Powder to Part*, 1st ed. Springer, New York, 2014.

[Book](#) [Google Scholar](#)

31. 31.

B.H. Toby, and R.B. Von Dreele, GSAS-II: The Genesis of a Modern Open-Source All Purpose Crystallography Software Package, *J. Appl. Crystallogr.*, 2013, **46**(2), p 544-549. <https://doi.org/10.1107/S0021889813003531>

[CAS](#) [Article](#) [Google Scholar](#)

32. 32.

C.A. Schneider, W.S. Rasband, and K.W. Eliceiri, NIH Image to ImageJ: 25 Years of Image Analysis, *Nat. Methods*, 2012, **9**(7), p 671-675. <https://doi.org/10.1038/nmeth.2089>

[CAS](#) [Article](#) [Google Scholar](#)

33. 33.

A.B. Murphy, Band-G
Application to Photoel
1337. <https://doi.org/10.1002/zaac.19784440119>

[CAS](#) [Article](#) [Google](#)

34. 34.

U.I. Gaya, *Heterogen*
2013.

SPRINGER NATURE

Help us improve your user experience

Would you be willing to answer a few questions about your experience using this site?

Provide Feedback

No Thanks

[Google Scholar](#)

35. 35.

H.Y. Deng, W.C. Hao, and H.Z. Xu, A Transition Phase in the Transformation from α -, β - And ϵ - to δ -Bismuth Oxide, *Chinese Phys. Lett.*, 2011, **28**(5), p 3-6. <https://doi.org/10.1088/0256-307X/28/5/056101>

[CAS](#) [Article](#) [Google Scholar](#)

36. 36.

F. Mou, C. Chen, J. Guan, D.R. Chen, and H. Jing, Oppositely Charged Twin-Head Electrospray: A General Strategy for Building Janus Particles with Controlled Structures, *Nanoscale*, 2013, **5**(5), p 2055-2064.

<https://doi.org/10.1039/c2nr33523a>

[CAS](#) [Article](#) [Google Scholar](#)

37. 37.

J. Hu, S. Zhou, Y. Sun, X. Fang, and L. Wu, Fabrication, Properties and Applications of Janus Particles, *Chem. Soc. Rev.*, 2012, **41**(11), p 4356-4378. <https://doi.org/10.1039/c2cs35032g>

[CAS](#) [Article](#) [Google Scholar](#)

38. 38.

P.E.A. Salomão, D.S. Gomes, E.J.C. Ferreira, F. Moura, L.L. Nascimento, A.O.T. Patrocínio, and M.C. Pereira, Photoelectrochemical Hydrogen Production from Water Splitting Using Heterostructured Nanowire Arrays of Bi₂O₃/BiAl Oxides as a Photocathode, *Sol. Energy Mater. Sol. Cells*, 2019, **194**, p 276-284.

<https://doi.org/10.1016/j.solmat.2018.12.037>

[CAS](#) [Article](#) [Google Scholar](#)

39. 39.

M.W. Kim, B. Joshi, E. Samuel, K. Kim, Y. Il Kim, T.G. Kim, M.T. Swihart, and S.S. Yoon, Highly Nanotextured β -Bi₂O₃ Pillars by Electrostatic Spray Deposition as Photoanodes for Solar Water Splitting, *J. Alloys Compd.*, 2018, **764**, p 881-889. <https://doi.org/10.1016/j.jallcom.2018.06.047>

[CAS](#) [Article](#) [Google Scholar](#)

40. 40.

H.Y. Jiang, K. Cheng, and J. Lin, Crystalline Metallic Au Nanoparticle-Loaded α -Bi₂O₃ Microrods for Improved Photocatalysis, *Phys. Chem. Chem. Phys.*, 2012, **14**(35), p 12114-12121.

<https://doi.org/10.1039>

[CAS](#) [Article](#) [Google](#)

41. 41.

G. Zhu, W. Que, and J. Lin, Synthesis of Janus Microspheres under V

<https://doi.org/10.1016>

[CAS](#) [Article](#) [Google](#)

42. 42.

SPRINGER NATURE

Help us improve your user experience

Would you be willing to answer a few questions about your experience using this site?

Provide Feedback

No Thanks

K. Yang, J. Li, Y. Peng, and J. Lin, Enhanced Visible Light Photocatalysis over Pt-Loaded Bi₂O₃: An Insight into Its Photogenerated Charge Separation, Transfer and Capture, *Phys. Chem. Chem. Phys. R. Soc. Chem.*, 2017, **19**(1), p 251-257. <https://doi.org/10.1039/c6cp06755g>

[CAS](#) [Article](#) [Google Scholar](#)

43. 43.

S.J.A. Moniz, S.A. Shevlin, D.J. Martin, Z.X. Guo, and J. Tang, Visible-Light Driven Heterojunction Photocatalysts for Water Splitting-a Critical Review, *Energy Environ. Sci. R. Soc. Chem.*, 2015, **8**(3), p 731-759. <https://doi.org/10.1039/c4ee03271c>

[CAS](#) [Article](#) [Google Scholar](#)

44. 44.

C. Li, J. Zhang, and K. Liu, A New Method of Enhancing Photoelectrochemical Characteristics of Bi/Bi₂O₃ Electrode for Hydrogen Generation via Water Splitting, *Int. J. Electrochem. Sci.*, 2012, **7**, p 5028-5034.

[CAS](#) [Google Scholar](#)

[Download references](#) ↓

Acknowledgments

The authors thank CONACYT for the financial support for master and Ph.D studies. This project was funded by CONACYT 293429 and 896 projects carried out at CENAPROT and LIDTRA national laboratories. The Francisco de Paula Santander University, Colombia, for funding in the mobility internship for research. The authors also thank Dr. Jesus Porcayo Calderón, CromoDuro y Horneados S.A. Especial thanks to Ariel Plaza Estrada for his technical support and feedback during the experimental setup.

Author information

Affiliations

1. Centro de Investigación y de Estudios Avanzados del Instituto Politécnico Nacional Unidad Querétaro, Libramiento Norponiente 2000, Fracc. Real de Juriquilla, C.P. 76230, Querétaro, Qro, México

M. T. Ayala-Ayala & J. Muñoz-Saldaña

2. Institut für Technische Chemie, Gottfried Wilhelm Leibniz Universität Hannover, Callinstrasse 3, 30167, Hannover, Germany

M. T. Ayala-Ayala

3. Universidad Francisco Santander, Colombia

M. Y. Ferrer-Pacheco

Authors

1. M. T. Ayala-Ayala
[View author publication](#)

SPRINGER NATURE

Help us improve your user experience

Would you be willing to answer a few questions about your experience using this site?

Provide Feedback

No Thanks

You can also search for this author in [PubMed](#) [Google Scholar](#)

2. M. Y. Ferrer-Pacheco

[View author publications](#)

You can also search for this author in [PubMed](#) [Google Scholar](#)

3. J. Muñoz-Saldaña

[View author publications](#)

You can also search for this author in [PubMed](#) [Google Scholar](#)

Corresponding author

Correspondence to [J. Muñoz-Saldaña](#).

Additional information

Publisher's Note

Springer Nature remains neutral with regard to jurisdictional claims in published maps and institutional affiliations.

Rights and permissions

[Reprints and Permissions](#)

About this article



Check for updates

Cite this article

Ayala-Ayala, M.T., Ferrer-Pacheco, M.Y. & Muñoz-Saldaña, J. Manufacturing of Photoactive β -Bismuth Oxide by Flame Spray Oxidation. *J Therm Spray Tech* **30**, 1107–1119 (2021). <https://doi.org/10.1007/s11666-021-01182-2>

[Download citation](#)

- Received: 28 August 2020
- Revised: 02 February 2021
- Accepted: 14 February 2021
- Published: 21 March 2021
- Issue Date: April 2021
- DOI: <https://doi.org/10.1007/s11666-021-01182-2>

Share this article

Anyone you share the following link with will be able to view this article.

SPRINGER NATURE

Help us improve your user experience

Would you be willing to answer a few questions about your experience using this site?

Provide Feedback

No Thanks

[Get shareable link](#)

Provided by the Springer Nature SharedIt content-sharing initiative

Keywords



- flame spray oxidation
- optical properties
- tetragonal bismuth oxide
- visible-light photocatalyst

[Download PDF](#) 

- [Sections](#)
- [Figures](#)
- [References](#)

- [Abstract](#)
- [Introduction](#)
- [Experimental Methods](#)
- [Results and Discussion](#)
- [Conclusions](#)
- [References](#)
- [Acknowledgments](#)
- [Author information](#)
- [Additional information](#)
- [Rights and permissions](#)
- [About this article](#)

Advertisement



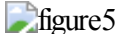
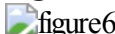
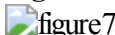
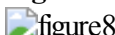
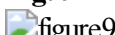
- **Fig. 1**
 figure1
[View in article](#)
- **Fig. 2**
 figure2
[View in article](#)

SPRINGER NATURE

Help us improve your user experience

Would you be willing to answer a few questions about your experience using this site?

[Provide Feedback](#)[No Thanks](#)

- **Fig. 3**

[View in articleFull size image](#) >
- **Fig. 4**

[View in articleFull size image](#) >
- **Figure 5**

[View in articleFull size image](#) >
- **Fig. 6**

[View in articleFull size image](#) >
- **Fig. 7**

[View in articleFull size image](#) >
- **Fig. 8**

[View in articleFull size image](#) >
- **Fig. 9**

[View in articleFull size image](#) >

1. H. Zhao, F. Tian, R. Wang, and R. Chen, A Review on Bismuth-Related Nanomaterials for Photocatalysis, *Rev. Adv. Sci. Eng.*, 2014, **3**(1), p 3-27.
<https://doi.org/10.1166/rase.2014.1050>

[Article](#) [Google Scholar](#)

2. D.A. Fernandez-Benavides, A.I. Gutierrez-Perez, A.M. Benitez-Castro, M.T. Ayala-Ayala, B. Moreno-Murguia, and J. Muñoz-Saldaña. Comparative Study of Ferroelectric and Piezoelectric Properties of Bi₂O₃-BT Ceramics near the Curie Temperature. *J. Am. Ceram. Soc.* (Basel), 2018, **11**(3), p 1000-1008.
<https://doi.org/10.3390/ceramics11031000>

[CAS Article](#) [Google Scholar](#)

3. D.A. Fernández-Benavides, A.I. Gutiérrez-Pérez, A.M. Jiménez, O.A. de Fuenmayor, B. Moreno-Murguía, J. Muñoz-Saldaña, A Novel Bismuth Oxide-Based Piezoelectric Transducer for Energy Harvesting. *Sensors*, 2020, **20**(12), p 3456-3468.
<https://doi.org/10.3390/s20123456>

SPRINGER NATURE

Help us improve your user experience

Would you be willing to answer a few questions about your experience using this site?

Provide Feedback

No Thanks

Quantification, *Sens. Actuators B Chem.*, 2019, **285**, p 423-430. <https://doi.org/10.1016/j.snb.2019.01.081>

[CAS Article](#) [Google Scholar](#)

4. M. Esquivel-Gaon, S. Anguissola, D. Garry, A.D.C. Gallegos-Melgar, J.M. Saldaña, K.A. Dawson, A. De Vizcaya-Ruiz, and L.M. Del Razo, Bismuth-Based Nanoparticles as the Environmentally Friendly Replacement for Lead-Based Piezoelectrics, *RSC Adv.*, 2015, **5**(35), p 27295-27304.

[CAS Article](#) [Google Scholar](#)

5. T. Jardiel, A.C. Caballero, and M. Villegas, Aurivillius Ceramics: Bi₄Ti₃O₁₂-Based Piezoelectrics, *J. Ceram. Soc. Jpn.*, 2008, **116**, p 511-518.

[CAS Article](#) [Google Scholar](#)

6. M. Mehring, From Molecules to Bismuth Oxide-Based Materials: Potential Homo- and Heterometallic Precursors and Model Compounds, *Coord. Chem. Rev.*, 2007, **251**(7-8), p 974-1006.

<https://doi.org/10.1016/j.ccr.2006.06.005>

[CAS Article](#) [Google Scholar](#)

7. G. Malmros, The Crystal Structure of Alpha-Bi₂O₃, *Acta Chem. Scand.*, 1970

<https://doi.org/10.3891/acta.chem.scand.24-0384>

[Article](#) [Google Scholar](#)

8. H.A. Harwig, On the Structure of Bismuthsesquioxide: The Alpha, Beta, Gamma and Delta-Phase, *Z. Anorg. Allg. Chem.*, 1978, **444**, p 151-166.

<https://doi.org/10.1090/gsm/146/03>

[CAS Article](#) [Google Scholar](#)

9. N. Cornei, N. Tancret, F. Abraham, and O. Mentré, New ϵ -Bi₂O₃ Metastable Polymorph, *Inorg. Chem.*, 2006, **45**(13), p 4886-4888.

<https://doi.org/10.1021/cr050000a001>

[CAS Article](#) [Google Scholar](#)

10. A.F. Gualtieri, S. Immo, X-Ray Diffraction Data of Compound ω -Bi₂O₃, *J. Solid State Chem.*, 1992, **92**, p 1-10.

[CAS Article](#) [Google Scholar](#)

SPRINGER NATURE

Help us improve your user experience

Would you be willing to answer a few questions about your experience using this site?

Provide Feedback

No Thanks

11. S. Ghedia, T. Locherer, R. Dinnebier, D.L.V.K. Prasad, U. Wedig, and M. Jansen, High-Pressure and High-Temperature Multianvil Synthesis of Metastable Polymorphs of Bi_2O_3 : Crystal Structure and Electronic Properties, *Phys. Rev. B*, 2010, **82**, p 1-12.
<https://doi.org/10.1103/PhysRevB.82.024106>

[CAS Article](#) [Google Scholar](#)

12. A.L.J. Pereira, O. Gomis, J.A. Sans, J. Contreras-García, F.J. Manjón, P. Rodríguez-Hernández, A. Muñoz, and A. Beltrán, β - Bi_2O_3 under Compression: Optical and Elastic Properties and Electron Density Topology Analysis, *Phys. Rev. B*, 2016, **93**(22), p 1-13.
<https://doi.org/10.1103/PhysRevB.93.224111>

[CAS Article](#) [Google Scholar](#)

13. A.L.J. Pereira, J.A. Sans, R. Vilaplana, O. Gomis, F.J. Manjón, P. Rodríguez-Hernández, A. Muñoz, C. Popescu, and A. Beltrán, Isostructural Second-Order Phase Transition of β - Bi_2O_3 at High Pressures: An Experimental and Theoretical Study, *J. Phys. Chem. C*, 2014, **118**(40), p 23189-23201.
<https://doi.org/10.1021/jp507826j>

[CAS Article](#) [Google Scholar](#)

14. X. Meng, and Z. Zhang, Bismuth-Based Photocatalytic Semiconductors: Introduction, Challenges and Possible Approaches, *J. Mol. Catal. A Chem*, 2016, **423**, p 533-549. <https://doi.org/10.1016/j.molcata.2016.07.030>

[CAS Article](#) [Google Scholar](#)

15. M. Schlesinger, S. Schulze, M. Hietschold, and M. Mehring, Metastable β - Bi_2O_3 Nanoparticles with High Photocatalytic Activity from Polynuclear Bismuth Oxide Clusters, *Dalt. Trans.*, 2013, **42**(4), p 1047-1056.
<https://doi.org/10.1039/c2dt32119j>

[CAS Article](#) [Google Scholar](#)

16. L. Liu, J. Jiang, S. Jin, Z. Xia, and M. Tang, Hydrothermal Synthesis of β - Bi_2O_3 Nanoparticles from Particles, *CrystE*, 2013, **1**, p 2532. <https://doi.org/10.1039/c3ce00011a>

[CAS Article](#) [Google Scholar](#)

17. J. Wang, X. Yang, K. Zhang, J. Wang, J. Deng, J. Chen, Fabrication of β - Bi_2O_3 Nanoparticles and Their Performance as Visible Light Photocatalysts, *Mater. Chem. A*, 2013, **1**, p 12345. <https://doi.org/10.1039/c3ta11652b>

SPRINGER NATURE

Help us improve your user experience

Would you be willing to answer a few questions about your experience using this site?

Provide Feedback

No Thanks

[CAS Article](#) [Google Scholar](#)

18. H.Y. Jiang, P. Li, G. Liu, J. Ye, and J. Lin, Synthesis and Photocatalytic Properties of Metastable β -Bi₂O₃ Stabilized by Surface-Coordination Effects, *J. Mater. Chem. A R. Soc. Chem.*, 2015, **3**(9), p 5119-5125.
<https://doi.org/10.1039/c4ta06235c>

[CAS Article](#) [Google Scholar](#)

19. T. Selvamani, S. Anandan, L. Granone, D.W. Bahnemann, and M. Ashokkumar, Phase-Controlled Synthesis of Bismuth Oxide Polymorphs for Photocatalytic Applications, *Mater. Chem. Front. R. Soc. Chem.*, 2018, **2**(9), p 1664-1673.
<https://doi.org/10.1039/c8qm00221e>

[CAS Article](#) [Google Scholar](#)

20. H.X. Hu, K.Q. Qiu, and G.F. Xu, Preparation of Nanometer δ - and β -Bismuth Trioxide by Vacuum Vapor-Phase Oxidation, *Trans. Nonferrous Met. Soc. China (English Ed.)*, 2006, **16**(1), p 173-177.
[https://doi.org/10.1016/S1003-6326\(06\)60031-9](https://doi.org/10.1016/S1003-6326(06)60031-9)

[CAS Article](#) [Google Scholar](#)

21. L. Kumari, J.H. Lin, and Y.R. Ma, Synthesis of Bismuth Oxide Nanostructures by an Oxidative Metal Vapour Phase Deposition Technique, *Nanotechnology*, 2007, **18**(29), p 7. <https://doi.org/10.1088/0957-4484/18/29/295605>

[CAS Article](#) [Google Scholar](#)

22. E. Diez, O. Monnereau, L. Tortet, G. Vacquier, P. Llewellyn, and F. Rouquerol, Synthesis of Bismuth (III) Oxide from Oxalate: A Study by Controlled Transformation Rate Thermal Analysis (CRTA), *J. Optoelectron. Adv. Mater.*, 2000, **2**(5), p 552-556.

[CAS](#) [Google Scholar](#)

23. Q. Huang, S. Zhang, C. Cai, and B. Zhou, β - and α -Bi₂O₃ Nanoparticles Synthesis by a Laser-Assisted Method and its Application towards the Degradation of Organic Pollutants, *J. Mater. Chem.*, 2011, **65**(6), p 988-995.
<https://doi.org/10.1016/j.jmcc.2011.05.011>

[CAS Article](#) [Google Scholar](#)

24. J. Hou, C. Yang, Z. Wang, and Y. Zhang, In Situ Synthesis of α -Bi₂O₃ Nanowires with Exceptional Photocatalytic Activity

SPRINGER NATURE

Help us improve your user experience

Would you be willing to answer a few questions about your experience using this site?

Provide Feedback

No Thanks

Performance, *Appl. Catal. B Environ.*, 2013, **142-143**, p 504-511. <https://doi.org/10.1016/j.apcatb.2013.05.050>

[CAS Article](#) [Google Scholar](#)

25. L. Pawlowski, *The Science and Engineering of Thermal Spray Coatings*, 2nd ed. Wiley, Hoboken, 2008.

[Book](#) [Google Scholar](#)

26. F. Fanicchia, D.A. Axinte, J. Kell, R. McIntyre, G. Brewster, and A.D. Norton, Combustion Flame Spray of CoNiCrAlY & YSZ Coatings, *Surf. Coatings Technol.*, 2017, **315**, p 546-557. <https://doi.org/10.1016/j.surfcoat.2017.01.070>

[CAS Article](#) [Google Scholar](#)

27. H.A. Harwig, and A.G. Gerards, The Polymorphism of Bismuth Sesquioxide, *Thermochim. Acta*, 1979, **28**(1), p 121-131. [https://doi.org/10.1016/0040-6031\(79\)87011-2](https://doi.org/10.1016/0040-6031(79)87011-2)

[CAS Article](#) [Google Scholar](#)

28. H.A. Harwig, and J.W. Weenk, Phase Relations in Bismuthsesquioxide, *ZAAC J. Inorg. Gen. Chem.*, 1978, **444**(1), p 167-177. <https://doi.org/10.1002/zaac.19784440119>

[CAS Article](#) [Google Scholar](#)

29. A.V. Naumov, World Market of Bismuth: A Review, *Metall. Rare Noble Met.*, 2007, **48**(1), p 13-19. <https://doi.org/10.3103/S1067821207010038>

[Article](#) [Google Scholar](#)

30. P.L. Fauchais, J.V.R. Heberlein, and M.I. Boulos, *Thermal Spray Fundamentals: From Powder to Part*, 1st ed. Springer, New York, 2014.

[Book](#) [Google Scholar](#)

31. B.H. Toby, and R.B. V
of a Modern Open-So
Software Package, *J. J*
544-549. <https://doi.org/10.1016/j.jcp.2007.05.002>

[CAS Article](#) [Google Scholar](#)

32. C.A. Schneider, W.S.
Image to ImageJ: 25 Y
Methods, 2012, **9**(7),
<https://doi.org/10.1038/nmeth.2007>

SPRINGER NATURE

Help us improve your user experience

Would you be willing to answer a few questions about your experience using this site?

Provide Feedback

No Thanks

[CAS Article](#) [Google Scholar](#)

33. A.B. Murphy, Band-Gap Determination from Diffuse Reflectance Measurements of Semiconductor Films, and Application to Photoelectrochemical Water-Splitting, *Sol. Energy Mater. Sol. Cells*, 2007, **91**(14), p 1326-1337. <https://doi.org/10.1016/j.solmat.2007.05.005>

[CAS Article](#) [Google Scholar](#)

34. U.I. Gaya, *Heterogeneous Photocatalysis Using Inorganic Semiconductor Solids*, Springer, Dordrecht, 2013.

[Google Scholar](#)

35. H.Y. Deng, W.C. Hao, and H.Z. Xu, A Transition Phase in the Transformation from α -, β - And ϵ - to δ -Bismuth Oxide, *Chinese Phys. Lett.*, 2011, **28**(5), p 3-6. <https://doi.org/10.1088/0256-307X/28/5/056101>

[CAS Article](#) [Google Scholar](#)

36. F. Mou, C. Chen, J. Guan, D.R. Chen, and H. Jing, Oppositely Charged Twin-Head Electrospray: A General Strategy for Building Janus Particles with Controlled Structures, *Nanoscale*, 2013, **5**(5), p 2055-2064. <https://doi.org/10.1039/c2nr33523a>

[CAS Article](#) [Google Scholar](#)

37. J. Hu, S. Zhou, Y. Sun, X. Fang, and L. Wu, Fabrication, Properties and Applications of Janus Particles, *Chem. Soc. Rev.*, 2012, **41**(11), p 4356-4378. <https://doi.org/10.1039/c2cs35032g>

[CAS Article](#) [Google Scholar](#)

38. P.E.A. Salomão, D.S. Gomes, E.J.C. Ferreira, F. Moura, L.L. Nascimento, A.O.T. Patrocínio, and M.C. Pereira, Photoelectrochemical Hydrogen Production from Water Splitting Using Heterostructured Nanowire Arrays of Bi₂O₃/BiAl Oxides as a Photocathode, *Sol. Energy Mater. Sol. Cells*, 2019, **194**, p 276-284. <https://doi.org/10.1016/j.solmat.2019.05.005>

[CAS Article](#) [Google Scholar](#)

39. M.W. Kim, B. Joshi, E. Kim, M.T. Swihart, and J. Kim, β -Bi₂O₃ Pillars by Electrodeposition as Photoanodes for Solar Water Splitting, *Chem. Mater.*, 2018, **30**(12), p 4050-4058. <https://doi.org/10.1021/acs.chemmater.8b01882>

[CAS Article](#) [Google Scholar](#)

SPRINGER NATURE

Help us improve your user experience

Would you be willing to answer a few questions about your experience using this site?

Provide Feedback

No Thanks

40. H.Y. Jiang, K. Cheng, and J. Lin, Crystalline Metallic Au Nanoparticle-Loaded α -Bi₂O₃ Microrods for Improved Photocatalysis, *Phys. Chem. Chem. Phys.*, 2012, **14**(35), p 12114-12121.

<https://doi.org/10.1039/c2cp42165h>

[CAS Article](#) [Google Scholar](#)

41. G. Zhu, W. Que, and J. Zhang, Synthesis and Photocatalytic Performance of Ag-Loaded β -Bi₂O₃ Microspheres under Visible Light Irradiation, *J. Alloys Compd.*, 2011, **509**(39), p 9479-9486.

<https://doi.org/10.1016/j.jallcom.2011.07.046>

[CAS Article](#) [Google Scholar](#)

42. K. Yang, J. Li, Y. Peng, and J. Lin, Enhanced Visible Light Photocatalysis over Pt-Loaded Bi₂O₃: An Insight into Its Photogenerated Charge Separation, Transfer and Capture, *Phys. Chem. Chem. Phys. R. Soc. Chem.*, 2017, **19**(1), p 251-257.

<https://doi.org/10.1039/c6cp06755g>

[CAS Article](#) [Google Scholar](#)

43. S.J.A. Moniz, S.A. Shevlin, D.J. Martin, Z.X. Guo, and J. Tang, Visible-Light Driven Heterojunction Photocatalysts for Water Splitting-a Critical Review, *Energy Environ. Sci. R. Soc. Chem.*, 2015, **8**(3), p 731-759. <https://doi.org/10.1039/c4ee03271c>

[CAS Article](#) [Google Scholar](#)

44. C. Li, J. Zhang, and K. Liu, A New Method of Enhancing Photoelectrochemical Characteristics of Bi/Bi₂O₃ Electrode for Hydrogen Generation via Water Splitting, *Int. J. Electrochem. Sci.*, 2012, **7**, p 5028-5034.

[CAS](#) [Google Scholar](#)

Over 10 million scientific documents at your fingertips

Switch Edition

- [Academic Edition](#)
- [Corporate Edition](#)
- [Home](#)
- [Impressum](#)
- [Legal information](#)
- [Privacy statement](#)
- [California Privacy Stat](#)
- [How we use cookies](#)
- [Manage cookies/Do not](#)
- [Accessibility](#)
- [FAQ](#)

SPRINGER NATURE

Help us improve your user experience

Would you be willing to answer a few questions about your experience using this site?

Provide Feedback

No Thanks

- [Contact us](#)
- [Affiliate program](#)

Not logged in - 181.235.49.74

Not affiliated

[Springer Nature](#) **SPRINGER NATURE**

© 2021 Springer Nature Switzerland AG. Part of [Springer Nature](#).

SPRINGER NATURE

Help us improve your user experience

Would you be willing to answer a few questions about your experience using this site?

Provide Feedback

No Thanks